JOC The Journal of Organic Chemistry

Article

pubs.acs.org/joc

Epoxy and Oxidoannulene Oxidation Mechanisms of Fused-Pentagon Chlorofullerenes: Oxides Linked by a Pirouette-Type Transition State

Qiao-Zhi Li,[†,‡] Jia-Jia Zheng,[‡] Ling He,[†] Xiang Zhao,*[,†] and Shigeru Nagase*[,‡]

[†]Institute for Chemical Physics and Department of Chemistry, School of Science, State Key Laboratory of Electrical Insulation and Power Equipment, Xi'an Jiaotong University, Xi'an 710049, China

[‡]Fukui Institute for Fundamental Chemistry, Kyoto University, Kyoto 606-8103, Japan

Supporting Information

ABSTRACT: Recently, the oxidative functionalization of double-fused-pentagon (DFP)-containing chlorofullerenes $^{\#271}C_{50}Cl_{10}$ and $^{\#913}C_{56}Cl_{10}$ was carried out, resulting in two monoepoxides with the oxygen atom added at the ortho site of pentalene on the DFP moiety. To uncover the reactivity of isolated-pentagon-rule violating fullerenes upon oxidation, two possible formation processes (ozone molecule and oxygen radical served as oxidation reagents) of these two oxides were systematically investigated through density functional theory calculations. For the ozone oxidation, two possible pathways were explored, and the results indicate that the biradical mechanism $Path_{os}$-RACDP is kinetically more favorable than $Path_{os}$-RABP, where R, A, and P represent reactants, ozonide intermediates, and oxidation products and B, C, and D represent another three oxygen-containing intermediates. The products obtained by ozone oxidation ([6,6]-55-closed epoxides P−C_3−C_{29} for $^{\#271}C_{50}Cl_{10}$ and P−C_{42}−C_{43} for $^{\#913}C_{56}Cl_{10}$ with oxygen atom added at the shortest and highest HOMO-contribution bonds) are consistent with experimental observations. However, the oxygen radical additions on these two chlorofullerenes favor generation of the [5,6]-66-open oxidoannulene adducts P−C_3−C_2 and P−C_{42}−C_{54}, respectively. Subsequent analyses of their geometrical features and structural stabilities suggest that these two oxidoannulene adducts are energetically unfavorable and could be converted to more stable epoxides mentioned above by undergoing a pirouette-type transition state. In these two diverse oxidation procedures, the favorable C−C bonds for ozone attacking and C atoms for oxygen-adsorption are rationalized in terms of their bond lengths and HOMO contributions as well as pyramidalization angles.

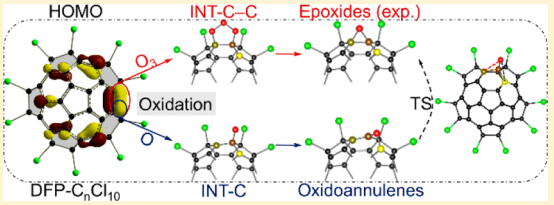

INTRODUCTION

Chemical functionalization of fullerenes, such as oxidation, has served as an efficient approach to modulate their electronic and physicochemical properties, making fullerene derivatives more promising for practical applications.[1−4] For example, the polymeric fullerene oxides of C_{60} and C_{70} are highly soluble in water, unlike pure C_{60} and C_{70}, providing considerable feasibility in water treatment.[3] In addition, fullerene oxides can be easily activated by a Lewis acid for further functionalization with various nucleophiles such as aromatic compounds, amines, and carbonyls.[5−8] It has been shown that in the presence of methanesulfonic acid (MsOH) fullerene oxide $C_{60}O$ could further react with cycloalkanones, resulting in the low-lying LUMO level of spiro-1,3-dioxolanofullerenes for an organic photovoltaic (OPV) cell.[8] Because of these valuable applications of fullerene oxides and their functionalized derivatives, efforts have been devoted to exploring and synthesizing various oxide species.[9−21] On one hand, fullerene oxides can be captured during the synthesis of fullerenes by arc-discharge or combustion,[9,10] such as the first reported fullerene oxide $C_{70}O$ which was detected in carbonaceous soot by the Diederich group in 1991.[9] In addition, ozonation of fullerenes and the subsequent ozonolysis were also widely employed to synthesize fullerene oxides. On the basis of this method, both [6,6]-closed epoxide and [5,6]-open oxidoannulene structures of $C_{60}O$ were obtained by thermolysis[16] and photolysis,[17] respectively. Similarly, several isomers of $C_{70}O$ were also obtained using this method.[18]

Unlike the great attention paid to the oxidation of above-mentioned isolated pentagon rule (IPR)-obeying fullerenes, oxidation of IPR-violating fullerenes[22,23] was scarcely involved in experiment until the recent synthesis of two chlorofullerene monoxides $^{\#271}C_{50}Cl_{10}O$ and $^{\#913}C_{56}Cl_{10}O$.[24] The carbon cages in these two oxides are both featured with a special double-fused-pentagon (DFP) moiety (Figure 1a and 1b). Structural characterization by crystallography and geometrical analyses indicate that both of these two oxides show an epoxy structure (closed epoxide) with the oxygen atom added at the ortho site of fused pentagons. This type of reactive site was also observed in Bingel−Hirsch reactions of IPR-violating fullerenes for C-addition.[25,26] For the convenience of discussion and understanding, we classify the nonequivalent C−C bonds of $^{\#271}C_{50}Cl_{10}$ and $^{\#913}C_{56}Cl_{10}$ into four types: bonds at the

Received: February 20, 2017
Published: June 7, 2017

DOI: 10.1021/acs.joc.7b00408
J. Org. Chem. 2017, 82, 6541−6549

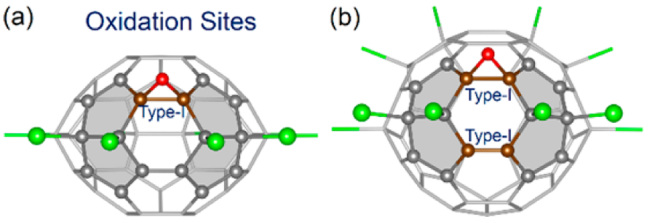

Figure 1. Structures of monoxides $^{\#271}C_{50}Cl_{10}O$ (a) and $^{\#913}C_{56}Cl_{10}O$ (b). The DFP moiety is represented by the ball-and-stick model. Atoms C, O, and Cl are colored in gray (brown for type-I bonds), red, and green, respectively.

ortho-site of fused pentagons are divided into type I (bonds on the DFP moiety) and type II (bonds next to the DFP moiety); the remaining bonds are divided into type III (without attaching chlorine atoms) and type IV (with one or two chlorine atoms attached). It is noted that these two oxidation sites both belong to the type-I bond. Thus, the superiority of these two type-I bonds over other three types of C−C bonds should be revealed in thermodynamics and kinetics. In addition, there exist two type-I bonds in $^{\#913}C_{56}Cl_{10}$ showing different oxidation abilities, which is also valuable for rationalization from the viewpoint of theoretical calculations.

In this work, we present our recent investigations on the oxidation mechanism of DFP-containing chlorofullerenes $^{\#271}C_{50}Cl_{10}$[27] and $^{\#913}C_{56}Cl_{10}$[28] through density functional theory computations. Since ozone molecule and oxygen radical could be generated in the UV irradiation of O_2,[29] these two species were considered as the oxidation reagents. Hence, the oxidation processes of $^{\#271}C_{50}Cl_{10}$ and $^{\#913}C_{56}Cl_{10}$ with ozone molecule and oxygen radical were investigated, respectively. The difference in the ability of nonequivalent C−C bonds for ozonation and that of nonequivalent C atoms for oxygen adsorption were uncovered from the viewpoints of thermodynamics and kinetics and then rationalized according to some intrinsic properties of chlorofullerenes. Finally, the rearrangement of adducts resulting from these two oxidation procedures was investigated.

COMPUTATIONAL METHODS

Full geometry optimizations of all relevant structures in the gas phase were carried out using the dispersion-corrected density functional theory method (U)M06-2X[30] with 6-31G(d) basis sets for all atoms. Subsequent frequency calculations were performed at the same level of theory to demonstrate the stationary points to be minimal for reactants, intermediates, and adducts or saddle points for transition states. Intrinsic reaction coordinate (IRC)[31−33] analyses were employed to confirm the transition states. Furthermore, single-point energy calculations were performed at the theory levels of (U)-B3LYP[34−36]/6-311G(d) and (U)B3LYP-D3[37]/6-311G(d) considering the solvent effect of toluene with the polarizable continuum model (PCM).[38]All calculations reported in this work were performed through the Gaussian 09 package.[39]

RESULTS AND DISCUSSION

Herein, the activity of C−C bonds for ozone attacking and that of C atoms for oxygen-adsorption as well as the relative stability of oxidation adducts is discussed at the (U)M06-2X/6-31G(d) level in the gas phase. In discussing the oxidation processes on those favorable reactive sites, we employed the results obtained by single-point calculations at the (U)B3LYP-D3/6-311G(d) level considering the solvent effect of toluene, which is more reliable in describing the biradical characters of the reaction species,[40,41] based on the structures optimized at the (U)M06-2X/6-31G(d) level. For convenience, it will be abbreviated as (U)B3LYP-D3/6-311G(d)//(U)M06-2X/6-31G(d). In addition, the Gibbs energies (298.15 K, 1 atm) are adopted in the discussion below unless otherwise noted.

Epoxy Oxidation of $^{\#271}C_{50}Cl_{10}$ and $^{\#913}C_{56}Cl_{10}$ via Ozonation and Thermolysis of Ozonides. Fullerene oxides such as $C_{60}O$ and $C_{70}O$ could be generally synthesized by the attack of ozone molecule to C−C bonds of fullerene cages, followed by the thermolysis of ozonides.[16−18] The corresponding oxidation mechanism has been theoretically simulated, but it was mainly concentrated on the ozonation and the first step of ozonolysis.[29,42] Here, a systematic and thorough reaction mechanism of this oxidation process was investigated for DFP-containing chlorofullerenes $^{\#271}C_{50}Cl_{10}$ and $^{\#913}C_{56}Cl_{10}$.

For the D_{5h}-symmetric $^{\#271}C_{50}Cl_{10}$ (Figure 2a), there are four nonequivalent C atoms and the corresponding six C−C bonds.

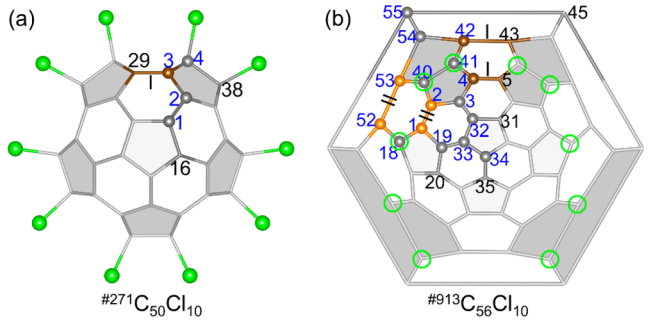

Figure 2. Molecular structure of $^{\#271}C_{50}Cl_{10}$ (a) and Schlegel diagram of $^{\#913}C_{56}Cl_{10}$ (b), including 4,16 nonequivalent carbon atoms represented by gray (brown and orange colors for atoms on type-I and type-II bonds) balls and the corresponding 6,25 C−C bonds, respectively. Sites attached with chlorine atoms in $^{\#913}C_{56}Cl_{10}$ are marked with green circles.

The existence of chlorine atoms on type IV bonds C_3−C_4 and C_4−C_{38} hinders the formation of their ozonides, leading to four possible ozonide intermediates (INT_A) for the ozonation of $^{\#271}C_{50}Cl_{10}$. At each ozonation site C_m−C_n, two conformers with the central O atom of ozone in front (INT_A-C_m−C_n-f) or back (INT_A-C_m−C_n-b) of the C_m−C_n bond were considered. The investigations on all possible structures of INT_A at low and high spin states (Supporting Information, Table S1) indicate that the singlet state is more stable than the triplet state by 22.0−52.8 kcal mol^{-1} (potential energies).In addition, calculations (Table 1 and also the Supporting Information, Figure S1) show that the most reactive site for ozone attacking is the [6,6]-55 bond C_3−C_{29}, the only type-I bond on DFP moiety, which results in two conformationally different ozonide intermediates INT_A-C_3−C_{29}-f and INT_A−C_3−C_{29}-b with relative energies of 0.0 and 2.8 kcal mol^{-1}, respectively. The second stable intermediate INT_A-C_1−C_2 is energetically higher than INT_A-C_3−C_{29}-f by up to24.0 kcal mol^{-1}. The corresponding transition states (TS_{RA}) from reactant to these three ozonide intermediates show that the energy barriers for the formation of INT_A-C_3−C_{29} with conformers -f and -b are identical and 4.1 kcal mol^{-1} lower than that of INT_A-C_1−C_2. These results suggest that the formation of ozonide intermediate INT_A-C_3−C_{29}-f is the most favorable both thermodynamically and kinetically with a high regioselectivity.

Previous theoretical calculations on $C_{70}O$ suggest that the best oxidation sites should depend on the most stable ozonide

DOI: 10.1021/acs.joc.7b00408
J. Org. Chem. 2017, 82, 6541−6549

Table 1. Relative Energies (E_{Rel}, kcal mol^{-1}) and Relative Gibbs Energies (G_{Rel}, kcal mol^{-1}) of Ozonide Intermediates (INT_A), the Corresponding Transition States (TS_{RA}), and the Final Oxidation Products (P) for $^{\#271}C_{50}Cl_{10}$ and $^{\#913}C_{56}Cl_{10}$ at the M06-2X/6-31G(d) Level[a]

							INT_A	TS_{RA}	ozonation[d]	P
$^{\#271}C_{50}Cl_{10}$	type 1	type 2	R_{C-C}	HOMO[b]	charge	POAV[c]	E_{rel}/ G_{rel}	G_{rel}	$\Delta G_{RA}^{\ddagger}$	G_{rel}
3−29f	I	[6,6]-55	1.371	11.05	0.031	9.36	0.0/0.0	0.2	5.5	0.0
3−29b	I	[6,6]-55	1.371	11.05	0.031	9.36	3.1/2.8	0.0	5.3	0.0
1−2	III	[6,6]-55	1.399	0.68	0.005	11.25	24.8/24.0	4.1	9.3	17.7
2−3f	III	[5,6]-66	1.430	(6.16)	0.022	9.80	34.5			16.6
							INT_A	TS_{RA}	ozonation[d]	P
$^{\#913}C_{56}Cl_{10}$	type 1	type 2	R_{C-C}	HOMO[b]	charge	POAV[c]	E_{rel}/ G_{rel}	G_{rel}	$\Delta G_{RA}^{\ddagger}$	G_{rel}
42−43b	I	[6,6]-55	1.357	12.42	0.034	9.57	0.0/0.0	0.0	4.0	0.0
4−5f	I	[6,6]-55	1.370	5.35	0.030	9.45	2.9/2.8	1.6	5.6	2.5
42−43f	I	[6,6]-55	1.357	12.42	0.034	9.57	3.0/2.7	0.5	4.5	0.0
4−5b	I	[6,6]-55	1.370	5.35	0.030	9.45	6.0/5.7	1.5	5.4	2.5
1−2f	II	[6,6]-55	1.369	1.15	0.032	9.10	9.8/9.8	3.5	7.4	5.5
1−2b	II	[6,6]-55	1.369	1.15	0.032	9.10	12.8/12.5	2.9	6.9	5.5
53−52f	II	[6,6]-56	1.396	(7.95)	0.016	6.98	24.9			18.7
3−4f	III	[5,6]-66	1.432	(3.08)	0.017	9.90	39.5			20.0
42−54f	III	[5,6]-66	1.443	(8.25)	0.018	9.44	49.1			24.0

[a]The bond lengths (R_{C-C}, Å), HOMO contributions (%), NBO charges (e), and pyramidalization angles (POAV, deg) on the C−C bonds of these two chlorofullerenes are also presented. Details for all nonequivalent C−C bonds are presented in the Supporting Information, Tables S1, S4, and S11. [b]The values in parentheses mean that the HOMO orbitals of these C−C bonds are symmetry-restricted to interact with the LUMO orbital of ozone molecule. [c]The average values of the two pyramidalization angles of carbon atoms of the C−C bond. [d]The Gibbs energy barriers ($\Delta G_{RA}^{\ddagger}$, kcal mol^{-1}) of ozonation additions on C−C bonds.

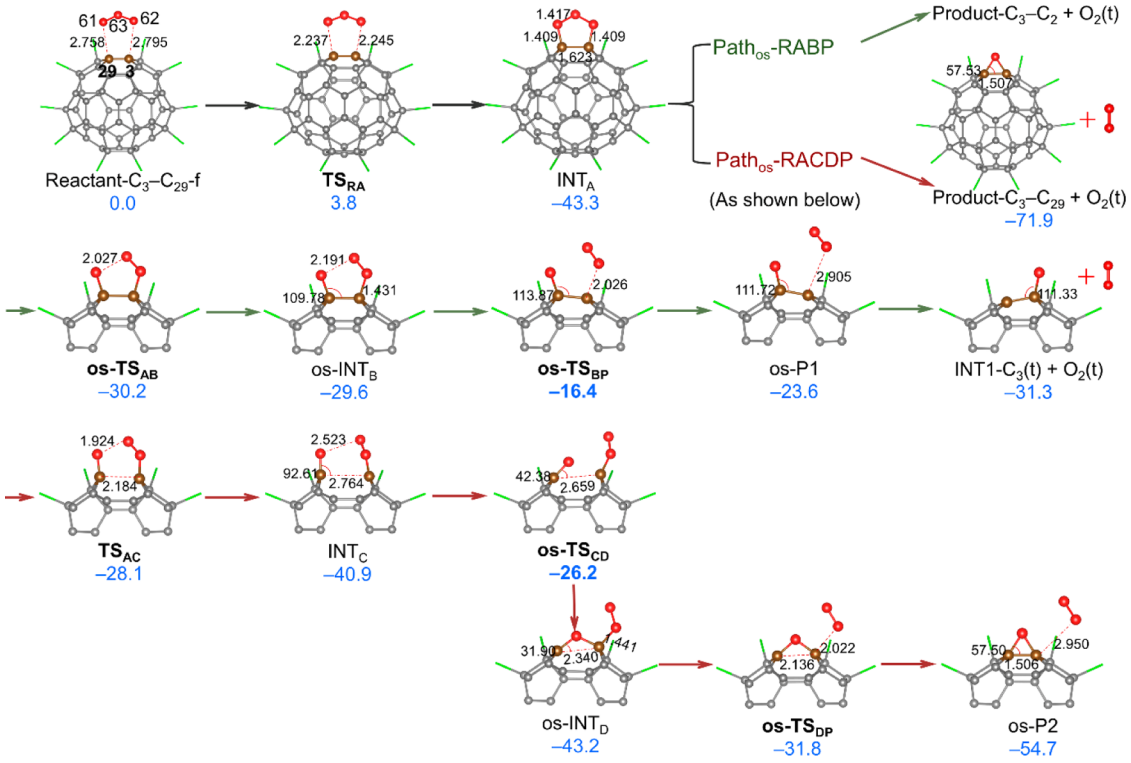

Figure 3. Ozone oxidation process of $^{\#271}C_{50}Cl_{10}$on the best addition site C_3−C_{29} at the (U)B3LYP-D3/6-311G(d)//(U)M06-2X/6-31G(d) level. Bond lengths (Å) and angles (deg) are marked in those relevant structures.

intermediates rather than the final oxidation adducts.[42] In addition, the thermolysis of ozonides to oxides by O_2 release should maintain the initial oxidation sites of ozonides to be consistent with the experimental results.[42] Consequently, the type-I bond C_3−C_{29} should be the best oxidation site in $^{\#271}C_{50}Cl_{10}$ because of its most stable and highly regioselective ozonide intermediate INT_A-C_3−C_{29}-f. This intermediate would lead to a closed epoxide P−C_3−C_{29} after thermolysis, which is in accordance with the experimentally observed product.[24] We further explored the thermolysis process of ozonide INT_A-C_3−C_{29}-f, which was not so straightforward because of the complexity in dealing with oxygen-containing intermediates

DOI: 10.1021/acs.joc.7b00408
J. Org. Chem. 2017, 82, 6541−6549

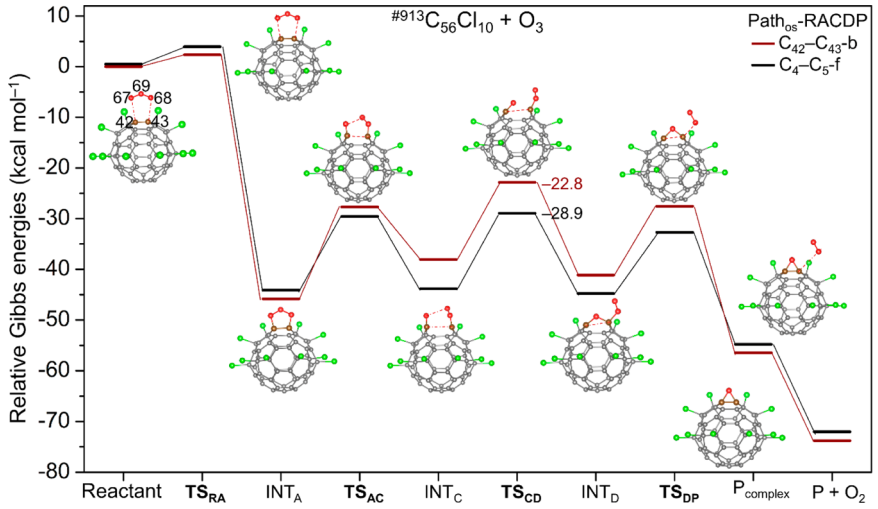

Figure 4. Gibbs energy profiles for the ozone oxidation of $^{\#913}C_{56}Cl_{10}$on sites C_{42}−C_{43} and C_4−C_5 at the(U)B3LYP-D3/6-311G(d)//(U)M06-2X/6-31G(d) level. Relevant structures on site C_{42}−C_{43} are also presented.

and transition states. As shown in Figure 3(see also the Supporting Information (Figure S2 and Tables S2 and S3) for full presentation of ozone oxidation process and the detailed discussion), three relevant intermediates INT_B, INT_C, and INT_D were obtained, affording two possible reaction pathways, Path-RABP and Path-RACDP, in which the open-shell singlet states (abbreviated as os) of relevant structures are more stable than the closed-shell singlet ones. Note that only one conformer could be formed for these three intermediates since atoms C_3 and C_{29} are equivalent. In the biradical pathway $Path_{os}$-RABP, the ozonide intermediate INT_A-C_3−C_{29}-f first dissociates into os-INT_B with the breaking of bond O_{61}−O_{63}, making this bond largely increase to 2.191 Å from 1.417 Å. Then, a complex os-P1 containing the removal of the O_{62}−O_{63} molecule is formed by going through the rate-determining transition state os-TS_{BP}. Calculations indicate that it is an endothermic process from INT_A-C_3−C_{29}-f to os-P1 with an activation barrier of 27.0 kcal mol^{-1}. In addition, the dissociated species from os-P1 turns out to be an oxygen-adsorption intermediate INT1-C_3, which finally leads to an oxidoannulene structure P−C_3−C_2 rather than the epoxide P−C_3−C_{29}, as will be discussed in oxygen radical addition of $^{\#271}C_{50}Cl_{10}$.

In comparison with the adduct P−C_3−C_2 formed in $Path_{os}$-RABP, the experimental product P−C_3−C_{29} is obtained by undergoing another biradical pathway $Path_{os}$-RACDP with the superiority of both thermodynamics and kinetics. In this process, both bonds O_{61}−O_{63} and C_3−C_{29} in the ozonide INT_A-C_3−C_{29}-f are broken to form an open-ring intermediate INT_C. A similar reaction process in the formation of $C_{70}O$ was previously reported by molecular dynamics (MD) simulations.[42] The bond lengths of O_{61}−O_{63} and C_3−C_{29} elongate from 1.417, 1.623 Å (INT_A) to 2.523, 2.764 Å (INT_C), respectively. The increase of these two bond lengths effectively decreases the steric hindrance for the subsequent bonding of O_{61}−C_3, resulting in the epoxide precursor os-INT_D. Finally, the closed epoxide P−C_3−C_{29} is obtained after the removal of oxygen molecule O_{62}−O_{63} and the simultaneous bonding of C_3−C_{29}. For this pathway, the calculated activation barrier (17.1 kcal mol^{-1} from INT_A-C_3−C_{29}-f to os-TS_{CD}) is 9.8 kcal mol^{-1} lower than that of $Path_{os}$-RABP. Thermodynamically, this ozonolysis process exhibits an exothermicity of 28.6 kcal mol^{-1}. We also attempted to locate the transition state for a one-step reaction from INT_C to P−C_3−C_{29}, but it turned out to be impractical. Therefore, the ozonolysis of INT_A-C_3−C_{29}-f to the experimental product P−C_3−C_{29} favors the biradical mechanism $Path_{os}$-RACDP by going through three transition states TS_{AC}, os-TS_{CD}, and os-TS_{DP}.

Similar to $^{\#271}C_{50}Cl_{10}$,the C_{2v}-symmetric $^{\#913}C_{56}Cl_{10}$ (Figure 2b), featured with 16 nonequivalent C atoms and the corresponding 25 C−C bonds, also exhibits high activities on type-I bonds (including C_{42}−C_{43} and C_4−C_5) to react with ozone molecule. As shown in Table 1 (see also the Supporting Information, Table S4 and Figure S3, for details of all C−C bonds), the formation of ozonide intermediate on the [6,6]-55 bond C_{42}−C_{43} is the most favorable from the viewpoint of both thermodynamics and kinetics. Subsequently, the thermolysis process of this lowest energy ozonide intermediate INT_A-C_{42}−C_{43}-b was investigated through two diverse reaction pathways like those in $^{\#271}C_{50}Cl_{10}$. As shown in Figure 4(see also the Supporting Information, Figure S4 and Table S5, for full presentation of ozone oxidation process),the rate-determining transition states in these pathways are consistent with those of $^{\#271}C_{50}Cl_{10}$. For $Path_{os}$-RABP, by going through an activation barrier of 27.0 kcal mol^{-1}, an oxygen-adsorption intermediate INT1-C_{42} will be obtained, which also leads to an open-ring structure P-C_{42}−C_{54} (see oxygen radical addition of $^{\#913}C_{56}Cl_{10}$). For $Path_{os}$-RACDP, the experimental product, closed epoxide P−C_{42}−C_{43}, will be generated with an activation barrier of 23.0 kcal mol^{-1}, suggesting that the ozonolysis of INT_A-C_{42}−C_{43}-b also favors a three-step biradical mechanism $Path_{os}$-RACDP with an energy release of 27.9 kcal mol^{-1}.

Except for the site C_{42}−C_{43}, another type-I bond C_4−C_5 is also favorable for reaction with the ozone molecule, forming the second stable ozonide intermediate INT_A-C_4−C_5-f (2.8 kcal mol^{-1} higher than INT_A-C_{42}−C_{43}-b) by going through the second lowest energy transition state TS_{RA}-C_4−C_5-f (1.6 kcal mol^{-1} higher than TS_{RA}-C_{42}−C_{43}-b). After the ozonolysis of INT_A-C_4−C_5-f under kinetically more favorable $Path_{os}$-RACDP, the corresponding closed epoxide P−C_4−C_5 is formed, which is thermodynamically unstable than P−C_{42}−C_{43} by 2.5 kcal mol^{-1}. It is noteworthy that the energy profile (Figure 4) shows that the ozonolysis of INT_A-C_4−C_5-f on the basis of $Path_{os}$-RACDP proceeds via energetically lower intermediates (INT_C and os-INT_D) and transition states (TS_{AC}, os-TS_{CD}, and os-

DOI: 10.1021/acs.joc.7b00408
J. Org. Chem. 2017, 82, 6541−6549

TS_{DP}) than that of INT_A-C_{42}−C_{43}-b.It seems that the former exhibits a faster ozonolysis rate than the latter. In consideration of the thermodynamically and kinetically more favorable ozonation process on bond C_{42}−C_{43} than bond C_4−C_5, we suggest that the formation of epoxides P−C_{42}−C_{43} and P−C_4−C_5 would be a competitive process. In comparison with Type-I bonds, Type-II (C_1−C_2 and C_{53}−C_{52}) and other bonds show a lower ozonation activity. For example, the ozonide intermediate INT_A-C_1−C_2-f and the corresponding transition state TS_{RA}-C_1−C_2-f for the third reactive bond C_1−C_2 are 9.8 and 3.5 kcal mol^{-1} higher than those for the bond C_{42}−C_{43}, respectively, which means that the formation of oxidation products on these bonds is less competitive.

On the basis of these analyses, we can conclude that the ozone oxidations of DFP-containing chlorofullerenes $^{\#271}C_{50}Cl_{10}$ and $^{\#913}C_{56}Cl_{10}$ will first undergo the ozonation process on type-I bonds C_3−C_{29} and C_{42}−C_{43}, respectively. The subsequent ozonolysis of INT_A-C_3−C_{29}-f and INT_A-C_{42}−C_{43}-b favors a three-step ($Path_{os}$-RACDP) rather than two-step ($Path_{os}$-RABP) process with a biradical mechanism, resulting in experimental products P−C_3−C_{29} and P−C_{42}−C_{43}, both featured with [6,6]-55-closed epoxy structures. The calculated activation barriers of $Path_{os}$-RACDP (17.1 and 23.0 kcal mol^{-1} from INT_A-C_3−C_{29}-f and INT_A-C_{42}−C_{43}-b to the corresponding rate-determining transition states os-TS_{CD}) suggest that the oxidation of these two chlorofullerenes by the ozone molecule would be practical at room temperature but with a slow kinetic character, which was also proposed in experiment.[24]

Oxidoannulene Oxidation via Oxygen Radical Reaction. Different from the [6,6]-55-closed epoxides P−C_3−C_{29}($^{\#271}C_{50}Cl_{10}$) and P−C_{42}−C_{43}($^{\#913}C_{56}Cl_{10}$) derived from the ozone oxidation process, the [5,6]-66-open oxidoannulene structures P−C_3−C_2 and P−C_{42}−C_{54} will be obtained through the triplet oxygen radical addition. Similar to those triplet carbene and nitrene radical reactions,[43,44] the oxygen radical will first attack carbon atoms of fullerenes to form energetically favorable oxygen-adsorption intermediates (INT1-C_i with oxygen adsorption on carbon atom C_i). For $^{\#271}C_{50}Cl_{10}$, since C_4 is attached with chlorine atom, its oxygen-adsorption intermediate cannot be formed. Calculations on other three possible intermediates INT1-C_i indicate that INT1-C_3 is the most stable with 8.0 kcal mol^{-1} lower than the second lowest energy INT1-C_1, as shown in Table 2 (see also the Supporting Information, Table S6, for details of all C atoms). Subsequently, the adsorbed oxygen in INT1-C_3 bonds with carbon atoms C_{29}, C_2, and C_4 to form three spin-conservation oxidation adducts, which then decay to their ground-state structures.[42] As shown in the Supporting Information, Table S7, calculations on these three corresponding oxidation adducts P−C_3−C_{29} (type I), P−C_3−C_2 (type III), and P−C_3−C_4 (type IV) demonstrate that the singlet state should be the ground state with 41.6, 38.5, and 52.6 kcal mol^{-1} lower than their triplet state structures, respectively. Unlike the singlet state with only one minimum for each adduct (closed-, open-, and open-ring geometries, respectively), two minima were located for their triplet state except for the type-IV adduct P−C_3−C_4, which has only the open-ring geometry. In addition, the open- (P−C_3−C_{29}) and closed-ring (P−C_3−C_2) geometries are 7.1 and 5.2 kcal mol^{-1} (potential energies) more favorable than their corresponding closed- and open-ring geometries, which was also discovered for $C_{70}O$.[42] On the basis of these results, our investigations on the subsequent bonding mechanism of O−$C_{29/2/4}$ will concentrate on the formation of spin-conservation triplet oxidation adducts P_t-C_3−C_{29}, P_t-C_3−C_2, and P_t-C_3−C_4 with open-, closed-, and open-ring geometries, respectively.

Table 2. Relative Energies (E_{Rel}, kcal mol^{-1}) and Relative Gibbs Energies (G_{Rel}, kcal mol^{-1}) of Oxygen-Adsorption Intermediates INT1-C_i for $^{\#271}C_{50}Cl_{10}$ and $^{\#913}C_{56}Cl_{10}$ at the UM06-2X/6-31G(d) Level[a]

$^{\#271}C_{50}Cl_{10}$	type	HOMO	POAV	E_{rel}/G_{rel}
3	566	5.58	9.36	0.0/0.0
1	566	0.10	12.24	8.6/8.0
2	566	0.58	10.25	16.6
$^{\#913}C_{56}Cl_{10}$	type	HOMO	POAV	E_{rel}/G_{rel}
42	566	6.21	9.57	0.0/0.0
4	566	2.68	9.45	2.6/2.6
53	566	7.59	7.42	2.7/2.6
2	566	0.95	9.24	5.8
54	566	2.03	9.30	17.2
52	666	0.36	6.54	17.5
3	566	0.41	10.35	20.1

[a]The HOMO contributions (%) and pyramidalization angles (POAV, deg) on the C atoms of these two chlorofullerenes are also presented. Details for all nonequivalent C atoms are presented in the Supporting Information, Table S6.

As shown in Figure 5 (see also the Supporting Information, Figure S5 and Table S8), the formation of P_t-C_3−C_2 from INT1-C_3 is a one-step process going through the transition state TS-C_3−C_2. In this process, the vibration of O−C_2 occurs with a decrease of the C_2−C_3−O angle from 104.83° (INT1-C_3) to 58.82° (P_t-C_3−C_2). However, the other two adducts P_t-C_3−C_{29} and P_t-C_3−$C_4$with open-ring geometries cannot be formed directly from INT1-C_3 via a one-step process. Additional intermediates INT2-C_3−C_{29} and INT2-C_3−C_4 are inevitable to generate the open-ring geometries, making bonds C_3−C_{29} and C_3−C_4 enlarge to 2.452 and 2.537 Å from 1.528 and 1.595 Å in INT1-C_3. By going through transition states TS2-C_3−C_{29} and TS2-C_3−C_4, the bonding of O−C_{29} and O−C_4 takes place to form those two adducts. Similar to the bonding of O−C_2, the angles of C_{29}−C_3−O (85.64°) and C_4−C_3−O (92.88°) in INT2 decrease to 32.93° and 35.39° in adducts, respectively. Since their activation barriers are, respectively, higher than that of P_t-C_3−C_2 by 17.0 (P_t-C_3−C_{29}) and 6.9 kcal mol^{-1} (P_t-C_3−C_4), we can conclude that the adsorbed oxygen in INT1-C_3 favors to further bond with atom C_2, leading to the final ground state (singlet) structure P_s-C_3−C_2, featured with an open oxidoannulene geometry.

For $^{\#913}C_{56}Cl_{10}$, 13 possible oxygen-adsorption intermediates were optimized, providing the most stable isomer INT1-C_{42} (Table 2 and also the Supporting Information, Table S6, for details of all C atoms). The subsequent bonding of O−$C_{43/54/41}$ from INT1-C_{42} can also result in three corresponding oxidation adducts. On the basis of their closed- and open-ring geometry calculations at both the singlet and triplet states (Supporting Information, Table S7), the formation processes of spin-conservation oxidation adducts P_t-C_{42}−C_{43} (type I), P_t-C_{42}−C_{54} (type III), and P_t-C_{42}−C_{41} (type IV) with open-, closed-, and open-ring geometries were further investigated like those for $^{\#271}C_{50}Cl_{10}$. As shown in Figure 6 (see also the Supporting Information, Figure S6 and Table S9), from INT1-C_{42} to P_t-C_{42}−C_{54}, only one transition state TS-C_{42}−C_{43} was located with a low activation barrier of 8.5 kcal mol^{-1}. On the other hand, to generate adducts P_t-C_{42}−C_{43} and P_t-C_{42}−C_{41} from INT1-C_{42}, one additional intermediate and two transition states

DOI: 10.1021/acs.joc.7b00408
J. Org. Chem. 2017, 82, 6541−6549

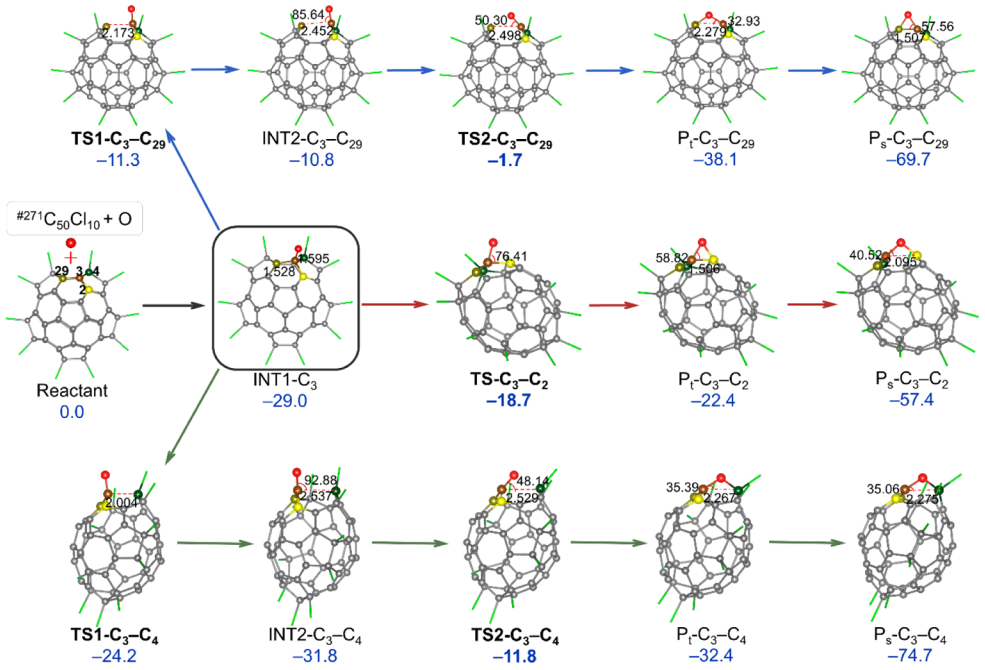

Figure 5. Oxygen radical oxidation process of $^{\#271}C_{50}Cl_{10}$ on the best oxygen-adsorption site C_3 at the (U)B3LYP-D3/6-311G(d)//(U)M06-2X/6-31G(d) level. Bond lengths (Å) and angles (deg) are marked in those relevant structures.

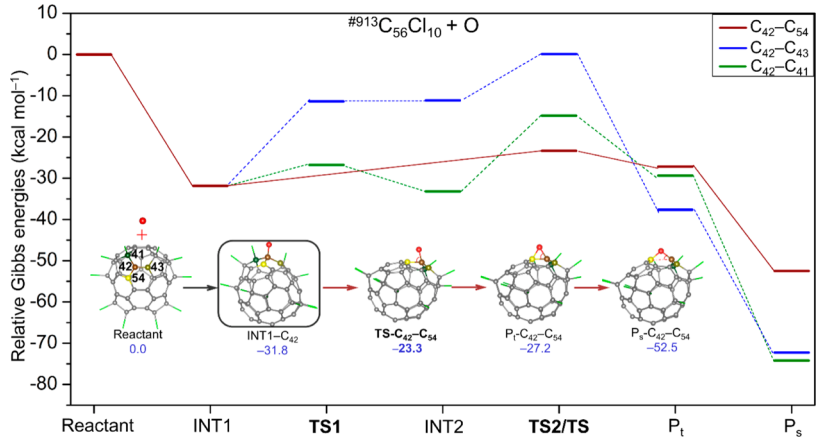

Figure 6. Gibbs energy profiles and relevant structures for oxygen radical oxidation of $^{\#913}C_{56}Cl_{10}$ on the best oxygen-adsorption site C_{42} at the (U)B3LYP-D3/6-311G(d)//(U)M06-2X/6-31G(d) level.

are still inevitable, which are similar to those of P_t-C_3–C_{29} and P_t-C_3–C_4 in the case of $^{\#271}C_{50}Cl_{10}$. The calculated barriers indicate that extra energies of 23.5 and 8.5 kcal mol^{-1} are required to obtain these two adducts compared to that of P_t-C_{42}–C_{54}. Therefore, the bonding of O–C_{54} from INT1-C_{42} is kinetically more favorable than that of O–C_{43} and O–C_{41}, resulting in an open oxidoannulene structure P_s-C_{42}–C_{54} in its ground state.

Except for the site C_{42}, another two sites C_4 and C_{53} (Table 2) also exhibit favorable activity of oxygen adsorption, and the formed intermediates INT1-C_4 and INT1-C_{53} are 2.6 kcal mol^{-1} higher than INT1-C_{42}. As presented in the Supporting Information, Figure S6 and Tables S7 and S9, like the site C_{42}, investigations on the bonding processes of O–$C_{5/3/41}$ for the site C_4 indicate that the formation of open oxidoannulene adduct P_s-C_4–C_3(type III) exhibits the lowest activation barrier of 10.2 kcal mol^{-1}, which is 15.2 and 5.9 kcal mol^{-1} more favorable than that of P_s-C_4–C_5 (type I) and P_s-C_4–C_{41} (type IV). For site C_{53}, the formation of spin-conservation oxidation adducts P_t-C_{53}–C_{54} (type III), P_t-C_{53}–C_{52} (type II), and P_t-C_{53}–C_{40} (type IV) with open-, closed-, and open-ring geometries were also investigated. Results indicate that the bonding of O–C_{52} from INT1-C_{53} is kinetically more favorable than that of O–C_{54} and O–C_{40} by 27.4 and 10.1 kcal mol^{-1}, respectively. In addition, for the formation of P_t-C_{53}–C_{54}, the breaking of C_{53}–C_{54} and the bonding of O–C_{54} could occur simultaneously without an additional intermediate INT2-C_{53}–C_{54}. We note that sites C_3 in $^{\#271}C_{50}Cl_{10}$ and C_{42}, C_4 in $^{\#913}C_{56}Cl_{10}$ all locate on type-I bonds and exhibit similar bonding mechanisms, whereas site C_{53} in $^{\#913}C_{56}Cl_{10}$ belongs to a type-II bond and shows a somewhat different mechanism, suggesting that the type of oxygen-adsorption sites may have some influence on the bonding mechanism.

As a consequence, for the oxygen radical addition of DFP-containing chlorofullerenes $^{\#271}C_{50}Cl_{10}$ and $^{\#913}C_{56}Cl_{10}$, the initial oxygen-adsorption addition occurs on the 566 sites C_3

DOI: 10.1021/acs.joc.7b00408
J. Org. Chem. 2017, 82, 6541–6549

and C_{42}, both located on type-I bonds. Then the bonding of $O-C_2$ and $O-C_{54}$ from the oxygen-adsorption intermediates INT1-C_3 and INT1-C_{42} is kinetically more favorable, resulting in the [5,6]-66-open oxidoannulene structures $P-C_3-C_2$ and $P-C_{42}-C_{54}$, respectively. The corresponding activation barriers (10.4 and 8.5 kcal mol^{-1}) suggest that this oxidation process could occur at room temperature.

Reasons for the Regioselectivity of Ozonation and Oxygen-Adsorption Processes. As discussed above, the key steps for ozone molecule and oxygen radical oxidations are the formation of ozonide intermediates (INT_A) and oxygen-adsorption intermediates (INT1-C_i), respectively, suggesting that the reactivities of ozonation on C−C bonds and oxygen-adsorption on C atoms play crucial roles in determining the oxidation sites. It is of considerable interest to rationalize the reactivities of addition sites in $^{\#271}C_{50}Cl_{10}$ and $^{\#913}C_{56}Cl_{10}$ by some of their inherent features. For this purpose, we first investigated the frontier orbitals of these two chlorofullerenes and the oxidation reagents. As shown in Figure 7 (see also the

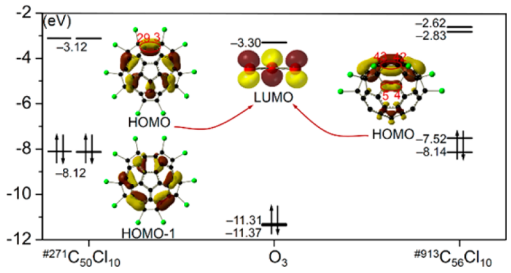

Figure 7. Diagram of the main frontier orbitals for chlorofullerenes ($^{\#271}C_{50}Cl_{10}$ and $^{\#913}C_{56}Cl_{10}$) and the oxidation reagent (ozone molecule).

Supporting Information, Table S10, for the detailed discussion), the calculated orbital energy gaps suggest that the orbital interaction should mainly occur between the HOMO of chlorofullerene and the LUMO of the oxidation reagent. In combination with the Woodward−Hoffmann rule[45] and frontier orbital theory,[46] it is suggested that C−C bonds and C atoms of chlorofullerenes with symmetry-allowed and larger HOMO contributions would be more reactive for the attack of an ozone molecule and oxygen radical, respectively. In addition, the C−C bond lengths, pyramidalization angles (the angle of the π-orbital axis vector, abbreviated as POAV),[47,48] and atomic charges are also important for the reactivity of fullerene and fullerene derivatives.[49,50] Generally, the electrophilic oxidation reagents (ozone molecule and oxygen radical) would favor attack of more negatively charged C−C bonds and C atoms. However, the calculated natural bond orbital (NBO)[51] charges show that those negatively charged C atoms are attached with chlorine atoms, and the effective C−C bonds for ozone attacking and C atoms for oxygen-adsorption are almost all positively charged in $^{\#271}C_{50}Cl_{10}$ and $^{\#913}C_{56}Cl_{10}$, suggesting that the atomic charge is unsuitable for discussing the oxidation reactivities of these two chlorofullerenes. Therefore, the following discussion will be mainly concentrated on the other three parameters.

As shown in Table 1 (see also the Supporting Information, Tables S1 and S4, for details of all C−C bonds), the type-I bonds C_3-C_{29} ($^{\#271}C_{50}Cl_{10}$) and $C_{42}-C_{43}$ ($^{\#913}C_{56}Cl_{10}$) possess the shortest bond lengths (1.371 and 1.357 Å) and the largest HOMO contributions (11.05% and 12.42%) with suitable orbital shapes, as reported previously,[24] affording their best reactivities in the ozonation process. For another favorable type-I bond C_4-C_5 ($^{\#913}C_{56}Cl_{10}$), it also exhibits a short bond length (1.370 Å) and a large HOMO contribution (5.35%). It is noteworthy that these three favorable bonds all exhibit small POAV values, indicating that the ozonation reactivities of C−C bonds mainly depend on their HOMO contributions (symmetry-allowed) and bond lengths. Accordingly, the poor ozonation reactivities of sites C_3-C_2 in $^{\#271}C_{50}Cl_{10}$ and $C_{42}-C_{54}$, C_4-C_3, $C_{53}-C_{52}$ in $^{\#913}C_{56}Cl_{10}$, which are favorable for the oxygen radical reaction, can be well rationalized by their symmetry-restricted HOMO orbital distributions and long bond lengths.

Similarly, the difference in oxygen-adsorption abilities of C atoms can also be rationalized according to these parameters, as shown in Table 2 (see also the Supporting Information, Table S6, for details of all C atoms). For instance, the best oxygen-adsorption ability of site C_3 in $^{\#271}C_{50}Cl_{10}$ can be attributed to its largest HOMO contribution (5.58%). For the best site C_{42} in $^{\#913}C_{56}Cl_{10}$, though its HOMO contribution (6.21%) is slightly smaller than that of site C_{53} with the largest contribution of 7.59%, it possesses a larger POAV angle than the latter one. It means that except for HOMO contribution, the pyramidalization angle also has some influence on oxygen-adsorption abilities of C atoms. Accordingly, the favorable reactivities of sites C_4 and C_{53} can be explained in a similar way. In addition, for sites C_3 and C_{52} in $^{\#913}C_{56}Cl_{10}$, which are geometrically possible for the formation of favorable oxygen radical oxidation adducts C_3-C_4 and $C_{52}-C_{53}$, their poor activities in oxygen-adsorption arise from their low HOMO contributions.

On the basis of the above analyses, the favorable C−C bonds for ozone attacking and C atoms for oxygen-adsorption can be well rationalized by some physical parameters of the pristine chlorofullerenes, including bond lengths, HOMO contributions, and pyramidalization angles. However, it is worth pointing out that the addition reactivities of C−C bonds and C atoms cannot be fully correlated with their physical parameters. For example, site C_{54} in $^{\#913}C_{56}Cl_{10}$ possesses a considerable HOMO contribution (2.03%) and POAV value (9.30), similar to site C_4, but it showed a poor oxygen-adsorption ability.

Rearrangement of Oxidoannulenes to Epoxides. Since the oxidation adducts from the ozone molecule and oxygen radical additions are different, we further investigated their relative stabilities to provide a better understanding on the oxidation processes of $^{\#271}C_{50}Cl_{10}$ and $^{\#913}C_{56}Cl_{10}$. As shown in Table 1 (see also the Supporting Information, Table S11, for details of all C−C bonds), the results indicate that the closed epoxides $P-C_3-C_{29}$ in $^{\#271}C_{50}Cl_{10}$ and $P-C_{42}-C_{43}$ in $^{\#913}C_{56}Cl_{10}$ are both the most stable adducts for addition sites without attaching chlorine atoms, which are 16.6 and 24.0 kcal mol^{-1} lower than the open oxidoannulene structures $P-C_3-C_2$ and $P-C_{42}-C_{54}$, respectively. A previous report suggests that the isomerization from the [6,6]- to the [5,6]-adduct in $C_{60}O$ could occur through a pirouette-type transition state,[52] which is also possible here according to the geometrical features of these adducts. As shown in Figure 8 (see also the Supporting Information, Figure S7), the corresponding transition states for the rearrangement of $P-C_3-C_2$ to $P-C_3-C_{29}$ and $P-C_{42}-C_{54}$ to $P-C_{42}-C_{43}$ were located, and the results indicate that open-shell singlet structures os-TS-$C_3-C_2-C_{29}$ and os-TS-$C_{42}-C_{54}-C_{43}$ are both energetically more favorable than their closed-shell

DOI: 10.1021/acs.joc.7b00408
J. Org. Chem. 2017, 82, 6541−6549

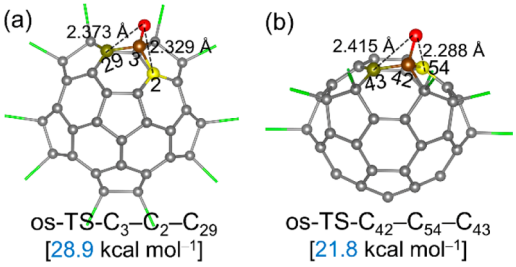

Figure 8. Optimized structures of transition states os-TS-C_3–C_2–C_{29} (a) and os-TS-C_{42}–C_{54}–C_{43} (b) for the rearrangement of P–C_3–C_2 to P–C_3–C_{29} in $^{\#271}C_{50}Cl_{10}$ and P–C_{42}–C_{54} to P–C_{42}–C_{43} in $^{\#913}C_{56}Cl_{10}$, respectively. The corresponding Gibbs energy barriers are also presented at the (U)B3LYP-D3/6-311G(d)//(U)M06-2X/6-31G(d) level.

singlet ones. The calculated activation barriers (28.9 and 21.8 kcal mol^{-1}, respectively) suggest that adducts P–C_3–C_2 ($^{\#271}C_{50}Cl_{10}$) and P–C_{42}–C_{54} ($^{\#913}C_{56}Cl_{10}$), derived from oxygen radical reaction, could be converted to more stable structures P–C_3–C_{29} and P–C_{42}–C_{43}(experimental products) under ambient conditions.

CONCLUSIONS

In summary, the oxidation mechanism of DFP-containing chlorofullerenes $^{\#271}C_{50}Cl_{10}$ and $^{\#913}C_{56}Cl_{10}$ was investigated by density functional theory calculations. First, we explored the process of ozonation and thermolysis of ozonides, which mainly depends on the activity of C–C bonds in binding with ozone molecule. It is revealed that the type-I bonds C_3–C_{29} in $^{\#271}C_{50}Cl_{10}$ and C_{42}–C_{43} in $^{\#913}C_{56}Cl_{10}$ are the most reactive, leading to ozonide intermediates INT_A-C_3–C_{29}-f and INT_A-C_{42}–C_{43}-b, respectively. The highest activities of these two bonds arise from their shortest bond lengths and highest HOMO contributions among all possible reaction sites. Subsequent investigations on the thermolysis of those two ozonides disclose one kinetically more favorable reaction pathway, $Path_{os}$-RACDP, over another one, $Path_{os}$-RABP (considering the biradical characters of relevant reaction species), resulting in experimentally obtained [6,6]-55-closed epoxides P–C_3–C_{29} and P–C_{42}–C_{43}, respectively. Calculations on the oxygen radical oxidation procedure indicate that carbon atoms C_3 ($^{\#271}C_{50}Cl_{10}$) and C_{42} ($^{\#913}C_{56}Cl_{10}$) show the best oxygen-adsorption abilities to form intermediates INT1-C_3 and INT1-C_{42}, also consistent with their highest HOMO contributions. Then, two [5,6]-66-open oxidoannulene structures P–C_3–C_2 and P–C_{42}–C_{54} could be obtained through the bonding of O–C_2 from INT1-C_3 and O–C_{54} from INT1-C_{42}, which are more favorable in kinetics than the formation of P–C_3–C_{29} and P–C_{42}–C_{43} after the bonding of O–C_{29} and O–C_{43} from these two intermediates. Nevertheless, these two open-ring adducts (P–C_3–C_2 and P–C_{42}–C_{54}) could be converted to the experimentally more stable closed-ring products (P–C_3–C_{29} and P–C_{42}–C_{43}), respectively, through the corresponding pirouette-type transition states. Therefore, both oxidation processes investigated here are possibly responsible for the formation of chlorofullerene oxides. Since the activation barriers are somewhat high, the oxidation of chlorofullerenes would proceed slowly under ambient conditions, as suggested by experiments.

ASSOCIATED CONTENT

Supporting Information

The Supporting Information is available free of charge on the ACS Publications website at DOI: 10.1021/acs.joc.7b00408.

Relative energies, physical parameters, and Cartesian coordinates of relevant structures for ozone molecule and oxygen radical oxidation processes of $^{\#271}C_{50}Cl_{10}$ and $^{\#913}C_{56}Cl_{10}$ (PDF)

AUTHOR INFORMATION

Corresponding Authors

*E-mail: xzhao@mail.xjtu.edu.cn.
*E-mail: nagase@ims.ac.jp.

ORCID

Xiang Zhao: 0000-0003-3982-4763

Notes

The authors declare no competing financial interest.

ACKNOWLEDGMENTS

This work was supported by the National Natural Science Foundation of China (21573172, 21503157, and 21503159), the National Key Basic Research Program of China (2012CB720904), the MOE Specialized Research Fund for the Doctoral Program of Higher Education of China (20130201110033), and the PhD Short-term Academic Visiting Program of China (40021136200002).

REFERENCES

(1) Cataldo, F.; Heymann, D. *Polym. Degrad. Stab.* **2000**, *70*, 237.
(2) Cataldo, F. *Carbon* **2002**, *40*, 1457.
(3) Strobel, P.; Ristein, J.; Ley, L. *J. Phys. Chem. C* **2010**, *114* (114), 4317.
(4) Wang, Z. Z.; Lu, Z. H.; Zhao, Y. L.; Gao, X. F. *Nanoscale* **2015**, *7*, 2914.
(5) Tajima, Y.; Hara, T.; Honma, T.; Matsumoto, S.; Takeuchi, K. *Org. Lett.* **2006**, *8*, 3203.
(6) Numata, Y.; Kawashima, J.; Hara, T.; Tajima, Y. *Chem. Lett.* **2008**, *37*, 1018.
(7) Tajima, Y.; Takeshi, K.; Shigemitsu, Y.; Numata, Y. *Molecules* **2012**, *17*, 6395.
(8) Mikie, T.; Saeki, A.; Ikuma, N.; Kokubo, K.; Seki, S. *Chem. Lett.* **2015**, *44*, 282.
(9) Diederich, F.; Ettl, R. *Science* **1991**, *252*, 548.
(10) Wood, J. M.; Kahr, B.; Hoke, S. H.; Dejarme, L.; Cooks, R. G.; Ben-Amotz, D. *J. Am. Chem. Soc.* **1991**, *113*, 5907.
(11) Creegan, K. M.; Robbins, J. L.; Robbins, W. K.; Millar, J. M.; Sherwood, R. D.; Tindall, P. J.; Cox, D. M.; McCauley, J. P., Jr; Jones, D. R. *J. Am. Chem. Soc.* **1992**, *114*, 1103.
(12) Taliani, C.; Ruani, G.; Zamboni, R.; Danieli, R.; Rossini, S.; Denisov, V. N.; Burlakov, V. M.; Negri, F.; Orlandi, G.; Zerbetto, F. *J. Chem. Soc., Chem. Commun.* **1993**, 220.
(13) Balch, A. L.; Costa, D. A.; Noll, B. C.; Olmstead, M. M. *J. Am. Chem. Soc.* **1995**, *117*, 8926.
(14) Smith, A. B.; Strongin, R. M.; Brard, L.; Furst, G. T.; Atkins, J. H.; Romanow, W. J.; Saunders, M.; Jiménez-Vázquez, H. A.; Owens, K. G.; Goldschmidt, R. J. *J. Org. Chem.* **1996**, *61*, 1904.
(15) Boltalina, O. V.; de La Vaissière, B.; Fowler, P. W.; Hitchcock, P. B.; Sandall, J. P.; Troshin, P. A.; Taylor, R. *Chem. Commun.* **2000**, 1325.
(16) Heymann, D.; Bachilo, S. M.; Weisman, R. B.; Cataldo, F.; Fokkens, R. H.; Nibbering, N. M.; Vis, R. D.; Chibante, L. F. *J. Am. Chem. Soc.* **2000**, *122*, 11473.
(17) Weisman, R. B.; Heymann, D.; Bachilo, S. M. *J. Am. Chem. Soc.* **2001**, *123*, 9720.

DOI: 10.1021/acs.joc.7b00408
J. Org. Chem. 2017, 82, 6541−6549

(18) Heymann, D.; Bachilo, S. M.; Weisman, R. B. *J. Am. Chem. Soc.* **2002**, *124*, 6317.
(19) Darwish, A. D.; Abdul-Sada, A. K.; Avent, A. G.; Street, J. M.; Taylor, R. *J. Fluorine Chem.* **2003**, *121*, 185.
(20) Yao, J. Y.; Yang, D. Z.; Xiao, Z.; Gan, L. B.; Wang, Z. M. *J. Org. Chem.* **2009**, *74*, 3528.
(21) Anderson, R. E.; Barron, A. R. *Dalton. Trans.* **2013**, *42*, 2186.
(22) Xu, X. F.; Shang, Z. F.; Wang, G. C.; Cai, Z. S.; Pan, Y. M.; Zhao, X. Z. *J. Mol. Struct.: THEOCHEM* **2002**, *589*, 265.
(23) Xu, X. F.; Xing, Y. M.; Yang, X.; Wang, G. C.; Cai, Z. S.; Shang, Z. F.; Pan, Y. M.; Zhao, X. Z. *Int. J. Quantum Chem.* **2005**, *101*, 160.
(24) Zhang, Z. Q.; Chen, S. F.; Gao, C. L.; Zhou, T.; Shan, G. J.; Tan, Y. Z.; Xie, S. Y.; Huang, R. B.; Zheng, L. S. *Inorg. Chem.* **2016**, *55*, 543.
(25) Garcia-Borràs, M.; Osuna, S.; Swart, M.; Luis, J. M.; Echegoyen, L.; Solà, M. *Chem. Commun.* **2013**, *49*, 8767.
(26) Li, Q. Z.; Zheng, J. J.; Zhao, X. *J. Phys. Chem. C* **2015**, *119*, 26196.
(27) Xie, S. Y.; Gao, F.; Lu, X.; Huang, R. B.; Wang, C. R.; Zhang, X.; Liu, M. L.; Deng, S. L.; Zheng, L. S. *Science* **2004**, *304*, 699.
(28) Tan, Y. Z.; Han, X.; Wu, X.; Meng, Y. Y.; Zhu, F.; Qian, Z. Z.; Liao, Z. J.; Chen, M. H.; Lu, X.; Xie, S. Y. *J. Am. Chem. Soc.* **2008**, *130*, 15240.
(29) Bulgakov, R. G.; Sabirov, D. S.; Dzhemilev, U. M. *Russ. Chem. Bull.* **2013**, *62*, 304.
(30) Zhao, Y.; Truhlar, D. G. *Theor. Chem. Acc.* **2008**, *120*, 215.
(31) Fukui, K. *J. Phys. Chem.* **1970**, *74*, 4161.
(32) Gonzalez, C.; Schlegel, H. B. *J. Chem. Phys.* **1989**, *90*, 2154.
(33) Gonzalez, C.; Schlegel, H. B. *J. Phys. Chem.* **1990**, *94*, 5523.
(34) Becke, A. D. *Phys. Rev. A: At., Mol., Opt. Phys.* **1988**, *38*, 3098.
(35) Lee, C.; Yang, W. T.; Parr, R. G. *Phys. Rev. B: Condens. Matter Mater. Phys.* **1988**, *37*, 785.
(36) Becke, A. D. *J. Chem. Phys.* **1993**, *98*, 5648.
(37) Grimme, S.; Antony, J.; Ehrlich, S.; Krieg, H. *J. Chem. Phys.* **2010**, *132*, 154104.
(38) Tomasi, J.; Mennucci, B.; Cammi, R. *Chem. Rev.* **2005**, *105*, 2999.
(39) Frisch, M. J.; Trucks, G. W.; Schlegel, H. B.; Scuseria, G. E.; Robb, M. A.; Cheeseman, J. R.; Scalmani, G.; Barone, V.; Mennucci, B.; Petersson, G. A.; Nakatsuji, H.; Caricato, M.; Li, X.; Hratchian, H. P.; Izmaylov, A. F.; Bloino, J.; Zheng, G.; Sonnenberg, J. L.; Hada, M.; Ehara, M.; Toyota, K.; Fukuda, R.; Hasegawa, J.; Ishida, M.; Nakajima, T.; Honda, Y.; Kitao, O.; Nakai, H.; Vreven, T.; Montgomery, J. A., Jr.; Peralta, J. E.; Ogliaro, F.; Bearpark, M.; Heyd, J. J.; Brothers, E.; Kudin, K. N.; Staroverov, V. N.; Keith, T.; Kobayashi, R.; Normand, J.; Raghavachari, K.; Rendell, A.; Burant, J. C.; Iyengar, S. S.; Tomasi, J.; Cossi, M.; Rega, N.; Millam, J. M.; Klene, M.; Knox, J. E.; Cross, J. B.; Bakken, V.; Adamo, C.; Jaramillo, J.; Gomperts, R.; Stratmann, R. E.; Yazyev, O.; Austin, A. J.; Cammi, R.; Pomelli, C.; Ochterski, J. W.; Martin, R. L.; Morokuma, K.; Zakrzewski, V. G.; Voth, G. A.; Salvador, P.; Dannenberg, J. J.; Dapprich, S.; Daniels, A. D.; Farkas, Ö.; Foresman, J. B.; Ortiz, J. V.; Cioslowski, J.; Fox, D. J. *Gaussian 09*, revision D.01; Gaussian, Inc.: Wallingford, CT, 2013.
(40) Cremer, D.; Crehuet, R.; Anglada, J. *J. Am. Chem. Soc.* **2001**, *123*, 6127.
(41) Olzmann, M.; Kraka, E.; Cremer, D.; Gutbrod, R.; Andersson, S. *J. Phys. Chem. A* **1997**, *101*, 9421.
(42) Bil, A.; Latajka, Z.; Morrison, C. A. *J. Phys. Chem. A* **2009**, *113*, 9891.
(43) Xu, Y. J.; Zhang, Y. F.; Li, J. Q. *J. Phys. Chem. C* **2007**, *111*, 3729.
(44) Dang, J. S.; Wang, W. W.; Nagase, S.; Zhao, X. *J. Phys. Chem. C* **2013**, *117*, 12882.
(45) Woodward, R. B.; Hoffmann, R. *Angew. Chem., Int. Ed. Engl.* **1969**, *8*, 781.
(46) Fukui, K. *Molecular Orbitals in Chemistry, Physics and Biology*; Löwdin, P. O., Pullman, B., Eds.; Academic Press: New York, 1964.
(47) Haddon, R. C. *Acc. Chem. Res.* **1988**, *21*, 243.
(48) Haddon, R. C. *J. Am. Chem. Soc.* **1990**, *112*, 3385.
(49) Garcia-Borràs, M.; Osuna, S.; Luis, J. M.; Swart, M.; Solà, M. *Chem. - Eur. J.* **2012**, *18*, 7141.
(50) Li, Q. Z.; Zheng, J. J.; Zhao, X. *Phys. Chem. Chem. Phys.* **2015**, *17*, 20485.
(51) Weinhold, F.; Landis, C. R. *Valency and Bonding: A Natural Bond Orbital Donor-Acceptor Perspective*; Cambridge University Press: New York, 2005.
(52) Sohn, W. Y.; Kim, T. W.; Lee, J. S. *J. Phys. Chem. A* **2010**, *114*, 1939.

DOI: 10.1021/acs.joc.7b00408
J. Org. Chem. 2017, 82, 6541−6549